Journal of Hazardous Materials 466 (2024) 133632

Contents lists available at ScienceDirect

Journal of Hazardous Materials

journal homepage: www.elsevier.com/locate/jhazmat

Research Paper

Pd-CeO_2 catalyst facilely derived from one-pot generated Pd@Ce-BTC for low temperature CO oxidation

Shaohua Xie [a,1], Wei Tan [a,b,1], Yuhan Xu [a,c], Chunying Wang [d], Yuan Feng [c], Kailong Ye [a], Lu Ma [e], Steven N. Ehrlich [e], Yaobin Li [d], Yan Zhang [d], Lin Dong [b], Jiguang Deng [c,*], Fudong Liu [a,f,**]

[a] Department of Civil, Environmental, and Construction Engineering, Catalysis Cluster for Renewable Energy and Chemical Transformations (REACT), NanoScience Technology Center (NSTC), University of Central Florida, Orlando, FL 32816, United States
[b] State Key Laboratory of Pollution Control and Resource Reuse, School of the Environment, Jiangsu Key Laboratory of Vehicle Emissions Control, School of Chemistry and Chemical Engineering, Center of Modern Analysis, Nanjing University, Nanjing 210023, China
[c] Beijing Key Laboratory for Green Catalysis and Separation, Key Laboratory of Beijing on Regional Air Pollution Control, Key Laboratory of Advanced Functional Materials, Education Ministry of China, Faculty of Environment and Life, Beijing University of Technology, Beijing 100124, China
[d] Center for Excellence in Regional Atmospheric Environment, Institute of Urban Environment, Chinese Academy of Sciences, Xiamen 361021, China
[e] National Synchrotron Light Source II (NSLS-II), Brookhaven National Laboratory, Upton, NY 11973, United States
[f] Department of Chemical and Environmental Engineering, University of California, Riverside, CA 92521, United States

HIGHLIGHTS

- A one-pot solvothermal method was developed for the preparation of Pd incorporated in Ce-BTC
- The Pd-CeO_2 catalyst derived from one-pot generated Pd@Ce-BTC exhibited superior CO oxidation activity
- The activity of the Pd-CeO_2 catalyst obtained through pyrolysis in nitrogen flow surpassed that obtained in air flow
- High Pd dispersion and rich surface Ce^{3+} species contributed to the improved CO oxidation activity on Pd-CeO_2

GRAPHICAL ABSTRACT

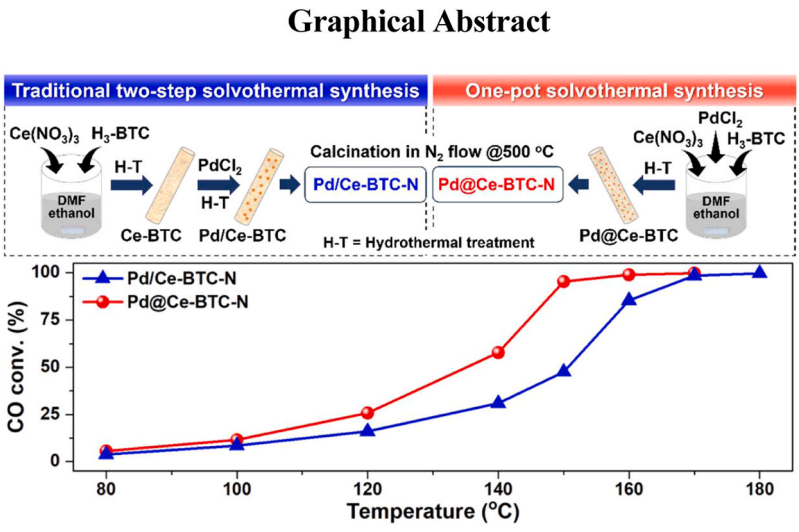

* Corresponding author.
** Corresponding author at: Department of Chemical and Environmental Engineering, University of California, Riverside, CA 92521, United States.
E-mail addresses: jgdeng@bjut.edu.cn (J. Deng), fudong.liu@ucr.edu (F. Liu).
[1] These authors contributed equally to this work

https://doi.org/10.1016/j.jhazmat.2024.133632
Received 19 November 2023; Received in revised form 14 January 2024; Accepted 25 January 2024
Available online 28 January 2024

ARTICLE INFO

Keywords:
Palladium catalyst
Ce-BTC
One-pot solvothermal method
CO oxidation
Surface Ce^{3+} species

ABSTRACT

Due to the capacity to offer abundant catalytic sites within porous solids featuring high surface areas, metal-organic frameworks (MOFs) and their derivatives have garnered considerable attention as prospective catalysts in environmental catalysis. To promote the industrial application of MOFs, there is an urgent need for an effective and environmental-friendly preparation approach. Breaking through the limitation of the traditional two-step preparation method that Pd was introduced to the already prepared Ce-BTC (Pd/Ce-BTC, BTC = 1, 3, 5 benzenetricarboxylate), in this work, we present a novel one-pot solvothermal method for synthesizing the Pd material supported by Ce-BTC (Pd@Ce-BTC). After pyrolysis in N_2 flow or air flow, Pd-CeO_2 catalysts derived from Pd@Ce-BTC exhibited much higher CO oxidation activity than those from Pd/Ce-BTC. Moreover, Pd/Ce-BTC and Pd@Ce-BTC pyrolyzed in N_2 flow (Pd/Ce-BTC-N and Pd@Ce-BTC-N) could better catalyze the oxidation of CO than Pd/Ce-BTC and Pd@Ce-BTC pyrolyzed in air flow (Pd/Ce-BTC-A and Pd@Ce-BTC-A). Further characterizations revealed that the abundant surface Ce^{3+} species, rich surface adsorbed oxygen species and superior redox properties were the main reasons for the superior CO oxidation activity of Pd@Ce-BTC-N.

1. Introduction

Due to their precisely controlled pore sizes, customizable structures, and adaptable surface functionalities, metal-organic frameworks (MOFs) have been widely applied in chemical, energy and environment-related fields [6]; [18]; [22]. Particularly, the abundant catalytic sites within high-surface-area porous structures and the remarkable stability of some MOFs and their derived materials have made them promising catalysts [9]; [14]; [28]. For instance, Ikuno *et al.* constructed Cu-oxo cluster catalysts stabilized in NU-1000 for catalyzing the oxidation of methane to methanol efficiently [11]. An *et al.* confined the ultra-small Cu/ZnO_x nanoparticles in UiO-bpy, which exhibited superior catalytic performance in the hydrogenation of CO_2 to methanol [1]. Recently, using MOFs and MOFs-derived materials in the environmental catalysis field has become a research hotspot. Among those MOFs materials, *M*-BTC (*M* = Mn, Ce, Cu, Fe, etc., BTC = 1, 3, 5 benzenetricarboxylate) has been widely used as important precursors in the preparation of catalysts for various catalytic oxidation reactions to eliminate CO, toluene, formaldehyde, and so on [2]; [4]; [16]; [24]; [34].

Platinum group metals (PGMs) catalysts supported by CeO_2 have been one of the most attractive catalyst groups in various catalytic oxidation reactions.[19]; [26]; [29]; [30]; [32]; [36] Their catalytic performance was highly dependent on the states of PGMs as well as the properties of CeO_2 supports. To further tap the potential of CeO_2, many strategies have been proposed to increase the surface area, control the specific morphology, engineer the surface oxygen vacancies and enhance the redox capability [31]. PGM catalysts on such fine-tuned CeO_2 support with proper metal-CeO_2 interactions, dispersion and electronic states might exhibit superior catalytic performance in different reactions. Known for the high surface area, the presence of nanosized cavities/open channels and relatively low cost, Ce-BTC has been recognized as an ideal precursor for synthesizing CeO_2-based catalysts with improved catalytic performance [4]; [7]; [8]; [13]; [24]; [34]. For instance, Pd/CeO_2 catalysts derived from tetragonal Ce-BTC exhibited a higher proportion of Pd^0 and featured smaller Pd nanoparticles. These characteristics resulted in the enhanced catalytic performance in CO oxidation [7]. Pd/quasi-Ce-BTC synthesized through N_2 pyrolysis possessed elevated concentrations of Ce^{3+} and Pd^0, which could promote the activation of oxygen, and thus resulting in the superior catalytic performance in toluene oxidation.[24] Typically, these catalysts were prepared through multiple steps, initially involving the synthesis of Ce-BTC followed by pretreatment or/and the metal loading processes. However, such a synthetic route was intricate, costly, and less environmental-friendly. In the preparation of Ce-BTC, dimethylformamide (DMF) was utilized as the solvent [35]. Additionally, it has been reported that DMF could be a reducing agent in the synthesis of precious metal particles, such as Pd [3]. These findings have inspired us to investigate the possibility of merging the preparation of MOFs with the simultaneous synthesis and incorporation of precious metal particles within the pore structures of MOFs. Through such a one-pot synthesis route, Ce-BTC supported metal catalysts could be obtained in one step.

In this study, we present a one-pot solvothermal synthesis method for the in-situ construction of Pd species within the pore structure of Ce-BTC, resulting in Pd@Ce-BTC. Serving as a reference, a conventional method involving the synthesis of Ce-BTC followed by the impregnation of Pd was used to prepare Pd/Ce-BTC. Both Pd@Ce-BTC and Pd/Ce-BTC materials were pyrolyzed in either N_2 flow or air flow at 500 °C before use. In comparison to the Pd/CeO_2 catalysts derived from conventional Pd/Ce-BTC, those prepared from one-pot synthesized Pd@Ce-BTC exhibited higher Pd dispersion and enhanced CO oxidation performance. Furthermore, pyrolysis in N_2 flow was found to better facilitate the formation of more surface Ce^{3+} and more surface-adsorbed oxygen species on Pd/CeO_2 catalysts derived from both Pd/Ce-BTC and Pd@Ce-BTC than pyrolysis in air flow. The developed one-pot solvothermal synthesis method proved to be not only straightforward, efficient, and environmental-friendly, but also capable of fabricating Pd/CeO_2 catalyst with superior catalytic performance in CO oxidation.

2. Materials and experimental methods

2.1. Catalyst preparation

Ce-BTC was synthesized through a solvothermal method reported elsewhere [35]. Typically, 10 mmol of cerium nitrate and 6.67 mmol of trimesic acid were added to 60 mL of DMF. After stirring at room temperature (RT) for 1 h, the solution was transferred to a Teflon-lined autoclave and heated at 100 °C for 24 h with stirring. Afterwards, the product was filtered once cooling to RT naturally, and washed with methanol and deionized water, followed by drying in vacuum at 60 °C for 12 h.

Pd/Ce-BTC was prepared by a solvothermal method. 2 g of as-prepared Ce-BTC was dispersed in 60 mL of DMF, followed by the addition of $PdCl_2$ solution (1 wt% Pd/CeO_2). After stirring at RT for 1 h, the solution was transferred to a Teflon-lined autoclave and heated at 140 °C for 6 h with stirring. Then, the product was filtered, washed with methanol and deionized water, and dried in vacuum at 60 °C for 12 h. For comparison purpose, Pd/CeO_2 was also prepared via the same method except using CeO_2 as support. The CeO_2 support was obtained by calcining cerium nitrate at 500 °C for 3 h.

Pd@Ce-BTC was prepared via a one-pot solvothermal method as illustrated in Scheme 1. Typically, 10 mmol of cerium nitrate, 6.67 mmol of trimesic acid, and $PdCl_2$ solution (1 wt% Pd/CeO_2) were sequentially added to 60 mL of DMF. After stirring for 1 h, the solution was transferred to a Teflon-lined autoclave and heated at 100 °C for 24 h, and then heated to 140 °C and kept for another 6 h with stirring. After cooling to RT naturally, the product was filtered, washed with methanol and deionized water, and vacuum-dried at 60 °C for 12 h.

Pd/Ce-BTC and Pd@Ce-BTC were set into a tube furnace and treated

in air or N_2 flow at 500 °C for 3 h, and the obtained samples were suffixed with "-A" or "-N", respectively. For comparison, the Pd@Ce-BTC powder was also treated in air or N_2 flow at 800 °C for 3 h, and the obtained samples were denoted as Pd@Ce-BTC-A800 or Pd@Ce-BTC-N800, respectively. Pd/CeO_2 reference was treated in air flow at 800 °C for 3 h as well, and the obtained catalyst was named as Pd/CeO_2-A800.

According to the results of inductively coupled plasma atomic emission spectroscopic (ICP-AES), the real mass ratio of Pd in Pd/CeO_2, Pd/Ce-BTC-A, Pd@Ce-BTC-A, Pd/Ce-BTC-N, and Pd@Ce-BTC-N to CeO_2 was 0.98, 0.95, 1.01, 0.97, and 0.93 wt.%, respectively.

2.2. Catalyst characterizations

The detailed descriptions of catalyst characterizations by X-ray diffraction (XRD), Scanning transmission electron microscopy (STEM), N_2 physisorption, X-ray photoelectron spectroscopy (XPS), X-ray absorption spectroscopy (XAS), CO temperature-programmed reduction (CO-TPR), O_2 temperature-programmed desorption (O_2-TPD), Raman spectroscopy, and thermal gravimetric analysis (TGA) techniques can be found in the **Supplementary material**.

2.3. Catalytic performance evaluation

CO oxidation test was carried out using a conventional fixed-bed flow reactor at atmospheric pressure. Prior to the test, a mixture of catalyst (50 mg) and SiC (0.25 g) was loaded into a quartz tube (inner diameter of 4 mm) and pretreated in 10% O_2/Ar flow at 250 °C for 30 min. The feeding gas (83.3 mL·min^{-1}) was composed of 1% CO and 20% O_2, using Ar as balance, corresponding to the weight hourly space velocity (WHSV) of 100,000 mL·g^{-1}·h^{-1}. The effluent gas was analyzed by mass spectrometer (MS) using the *m/z* of 28, 44 and 32 for CO, CO_2 and O_2, respectively. The CO conversion (X_{CO}) and reaction rate (r) on Pd catalysts were calculated according to the following equations:

$$X_{CO}\ (\%) = \frac{[CO]_{in} - [CO]_{out}}{[CO]_{in}} \times 100\%$$

$$r\ (\mu mol \cdot g_{Pd}{}^{-1} \cdot s^{-1}) = \frac{F_{CO,in} \times X_{CO}}{m_{Pd}}$$

where $[CO]_{in}$ and $[CO]_{out}$ are the inlet and outlet concentrations of CO, $F_{CO,\,in}$ is the molar flow rate of CO, X_{CO} is the CO conversion, and m_{Pd} is the real mass of Pd in the catalysts.

3. Results and discussion

3.1. Structural characteristics

As depicted in **Fig. S1**, similar XRD patterns were observed on Ce-BTC and Pd@Ce-BTC, which could be well indexed to standard Ce-BTC structure as reported.[7] In consistence with Ce-BTC, Pd@Ce-BTC showed type IV isotherms (IUPAC classification) with H3-type hysteresis (**Fig. S2a**). These similar XRD patterns and N_2 adsorption-desorption isotherm plots for Ce-BTC and Pd@Ce-BTC indicated that the Pd species have been successfully introduced into Ce-BTC without damaging its structure via this developed one-pot solvothermal method, although the pore distribution of them was slightly different (**Fig. S2b**). The thermal stability and the weight loss characteristics for Ce-BTC and Pd@Ce-BTC were investigated by thermogravimetric analysis (TGA). As shown in **Fig. S3a**, the thermal degradation of Ce-BTC in the air flow exhibited three distinct rapid weight loss phases within the temperature range of 40–800 °C. The initial weight loss below 100 °C could be attributed to the loss of adsorbed and lattice-coordinated water. Subsequently, from 100 to 350 °C, the second weight loss could be ascribed to the desorption and oxidation of organic solvents. Lastly, the third weight loss, occurring between 350 and 800 °C, was likely associated with the combustion of the organic ligand within Ce-BTC.[9] When subjected to the N_2 flow environment, Ce-BTC exhibited two primary weight loss steps. The initial weight loss, occurring at temperatures below 500 °C, could be attributed to the desorption of water and organic solvents. Beyond 500 °C, the second step corresponded to the decomposition of organic ligand within Ce-BTC. The thermal weight loss profile of Pd@Ce-BTC closely paralleled with that of Ce-BTC in both air flow and N_2 flow, but with an overall lower weight loss (**Figs. S3b** and **S3c**). Based on the TGA results, the loading of Pd on the resulted Pd/CeO_2 catalysts for CO oxidation were precisely controlled at *ca.* 1 wt.%.

The XRD patterns (Fig. 1**a**) for all supported Pd/CeO_2 catalysts could be attributed to the cubic fluorite CeO_2 (JCPDF No. 34–0394). Comparing to the samples obtained in air flow, the XRD peaks of Pd/Ce-BTC-N and Pd@Ce-BTC-N obtained in N_2 flow displayed broader full width at half maximum (FWHM) of the peak, indicating the lower crystallinity of CeO_2. It should be noted that there was a shift to lower angles in the XRD peaks for Pd@Ce-BTC-N and Pd@Ce-BTC-A compared to those observed for Pd/CeO_2 and Pd/Ce-BTC-A (**Fig. S4**). This shift indicates a lattice expansion of CeO_2 due to the presence of abundant Ce^{3+} species in the catalysts prepared using the one-pot solvothermal method, potentially benefiting the CO oxidation. The lattice expansion was further confirmed by the calculated lattice parameters of 0.543 nm for Pd@Ce-BTC-N and 0.542 nm for Pd@Ce-BTC-A, in contrast to 0.541 nm for Pd/CeO_2 and Pd/Ce-BTC-A. Comparing to Pd@Ce-BTC-N, the much weaker XRD peaks on Pd/Ce-BTC-N should be due to the incomplete deligandation during the pyrolysis in N_2 flow. The

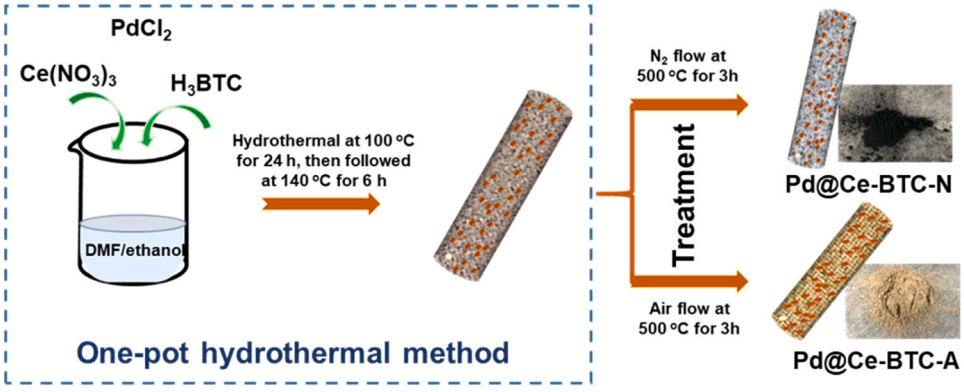

Scheme 1. Schematic diagram of synthesizing Pd@Ce-BTC catalysts using a one-pot hydrothermal method.

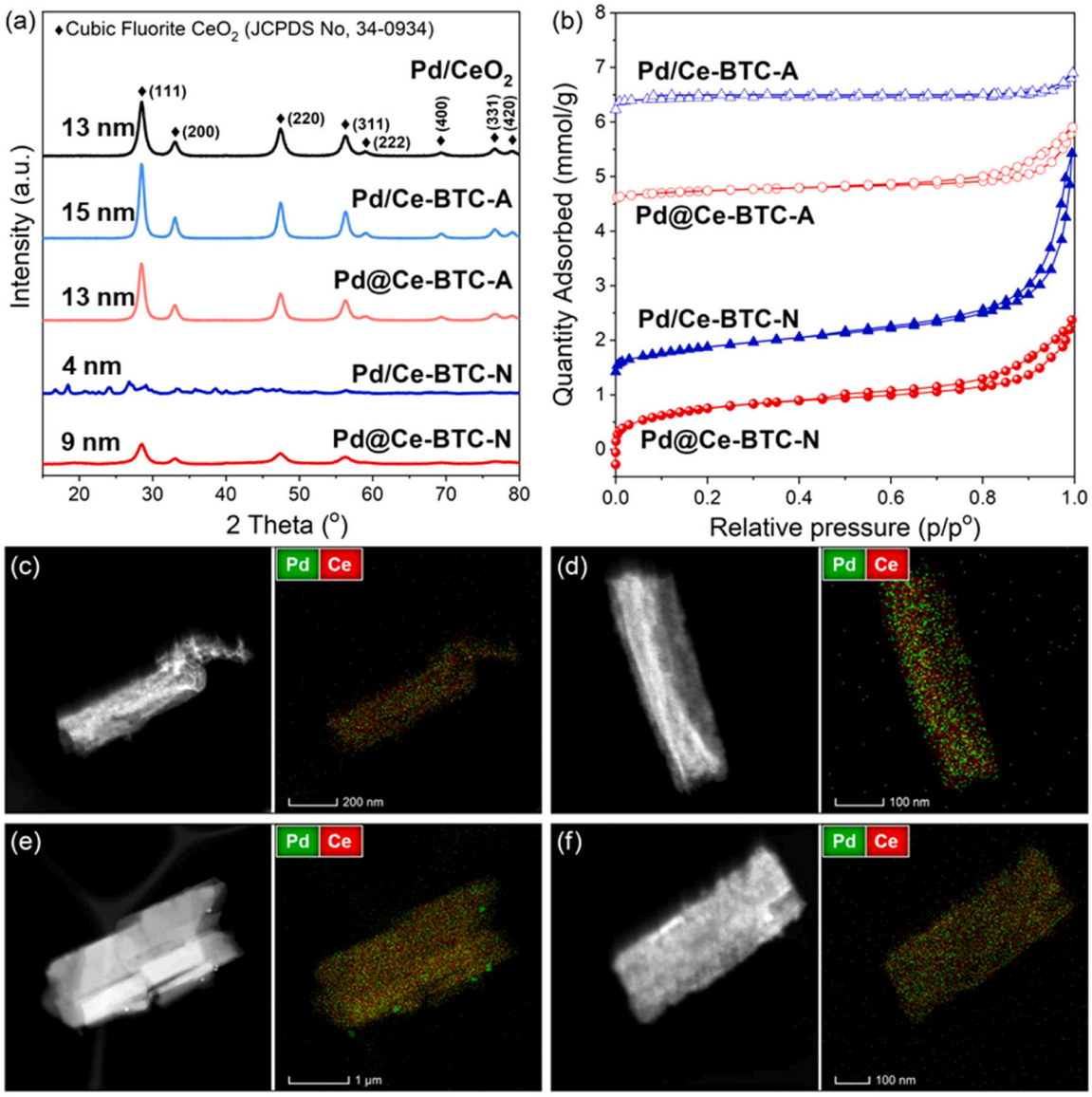

Fig. 1. (a) XRD patterns and (b) N_2 adsorption-desorption isotherms for Pd catalysts; HAADF-STEM and EDS-mapping images for (c) Pd/Ce-BTC-A, (d) Pd@Ce-BTC-A, (e) Pd/Ce-BTC-N, and (f) Pd@Ce-BTC-N. The CeO_2 crystalline sizes within the catalysts are inserted in Fig. 1**a**.

crystalline size of CeO_2 was further calculated using Scherrer equation for confirmation. As inserted in Fig. 1**a**, the crystalline sizes of CeO_2 in Pd/Ce-BTC-N (4 nm) and Pd@Ce-BTC-N (9 nm) were indeed much smaller than that in Pd/Ce-BTC-A (15 nm) and Pd@Ce-BTC-A (13 nm), respectively. The results of XRD were further supported by the Raman spectra (**Fig. S5**), with lower intensity of the bands assigned to CeO_2 F_{2g} mode observed on Pd/Ce-BTC-N and Pd@Ce-BTC-N, which was usually related to the lower crystallinity of CeO_2.([17]) These results suggested that the calcination in N_2 flow could benefit lowering the crystallinity of catalysts derived from Pd@Ce-BTC and Pd/Ce-BTC. As illustrated in Fig. 1**b**, through the measurement of N_2 adsorption-desorption isotherms, it was found that all catalysts exhibited IV isotherms with H3 hysteresis loops, suggesting the presence of mesoporous structure, which was confirmed by the results of the pore size distribution (**Fig. S6**). It was also found that higher specific surface area was achieved on the samples derived from the pyrolysis of precursors in N_2 flow (**Table S1**), especially for Pd@Ce-BTC-N (100 $m^2 \cdot g^{-1}$).

To further investigate the structure of the prepared catalysts, HAADF-STEM and EDS-mapping images were collected. As shown in Figs. 1**c**-1**f**, all catalysts were in short rod shape, and the size of CeO_2 rod in Pd@Ce-BTC-A and Pd@Ce-BTC-N was smaller than that in Pd/Ce-BTC-A and Pd/Ce-BTC-N. Moreover, it was noticeable that more uniformly distributed Pd species were formed on Pd@Ce-BTC-N comparing to that on Pd/Ce-BTC-N. Much smaller Pd clusters could also be observed by HR-TEM images (**Fig. S7**). The observations above suggested that the one-pot solvothermal synthesis method could significantly decrease the size of CeO_2 support and facilitate the dispersion of Pd species.

3.2. *Catalytic performance*

As a probe reaction, CO oxidation was used to evaluate the catalytic oxidation performance of the developed Pd-CeO_2 catalysts derived from Pd-Ce-BTC materials. As shown in Fig. 2**a**, the catalysts derived from both Pd/Ce-BTC and Pd@Ce-BTC performed much better than the conventional Pd/CeO_2 catalyst in CO oxidation reaction, hinting at the superiority of using Ce-BTC as the CeO_2 precursor. Moreover, the catalysts derived from Pd@Ce-BTC exhibited higher activity comparing to those from Pd/Ce-BTC, underscoring the advantageous impact of the one-pot solvothermal synthesis method on enhancing the catalytic

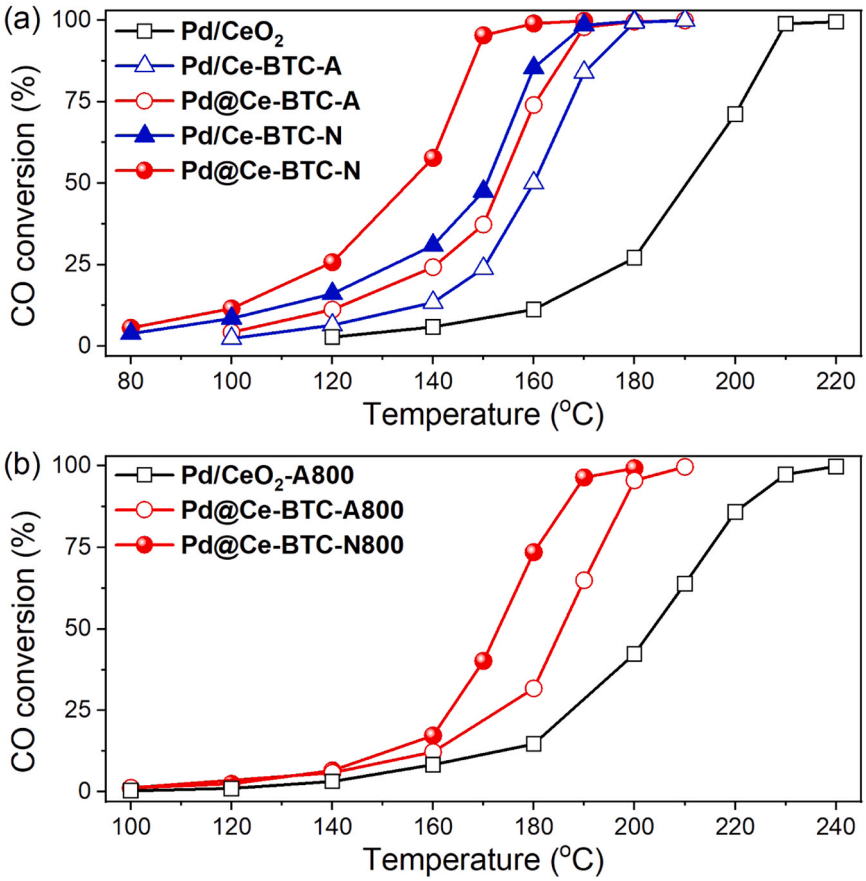

Fig. 2. CO oxidation activity on (a) Pd/CeO_2, Pd/Ce-BTC-A, Pd@Ce-BTC-A, Pd/Ce-BTC-N, and Pd@Ce-BTC-N catalysts. CO oxidation activity on (b) Pd/CeO_2-A800, Pd@Ce-BTC-A800, and Pd@Ce-BTC-N800 catalysts.

activity of Pd. Among all the catalysts, Pd@Ce-BTC-N exhibited the highest CO oxidation activity (with $T_{50} = 135$ °C, T_{50} was the temperature at which CO conversion reached 50%). In addition, the pyrolysis atmosphere had a notable influence on the CO oxidation activity of both Pd/Ce-BTC and Pd@Ce-BTC catalysts. Notably, the catalysts pyrolyzed in N_2 flow showed higher CO oxidation activity comparing to those pyrolyzed in air flow. In comparison to the recently reported Pd-CeO_2 catalysts prepared by various methods including impregnation, the Pd@Ce-BTC-N catalyst developed in this study demonstrated superior performance (**Table S2**). The catalytic stability and thermal stability of a catalyst are crucial for various operations, particularly for those conducted under high engine loads [19]. Therefore, two rounds of activity testing were conducted on both Pd/Ce-BTC-N and Pd@Ce-BTC-N catalysts, revealing superior catalytic stability with no observable decrease in CO oxidation activity (**Fig. S8**). To further assess the thermal stability and validate the advantages of pyrolysis in N_2 flow, Pd@Ce-BTC catalysts pyrolyzed in both N_2 and air flows at a high temperature of 800 °C for 3 h were obtained and evaluated for CO oxidation activity. It was evident that Pd@Ce-BTC-N800 exhibited higher CO oxidation activity than Pd@Ce-BTC-A800 (Fig. 2**b**). Moreover, Pd@Ce-BTC-A800 exhibited much higher CO oxidation activity than Pd/CeO_2-A800, indicating the satisfactory stability of the catalysts derived from Pd@Ce-BTC.

3.3. Oxidation states and local structure of Pd

The oxidation state and local structure of Pd species on all catalysts could be determined by the Pd K-edge XAS results (Fig. 3**, S9 and S10**). As depicted in Fig. 3**a**, the Pd K-edge XANES patterns of Pd@Ce-BTC-N, Pd/Ce-BTC-N, Pd/Ce-BTC-A, and Pd/CeO_2 catalysts were very similar to that of Pd foil, suggesting that the Pd species in these catalysts were mainly in metallic state. In contrast, the XANES pattern of Pd@Ce-BTC-A was a mixture of both Pd foil and PdO references, indicating that Pd species in Pd@Ce-BTC-A were partially in metallic state and partially in ionic state. It was further calculated by the XANES linear combination fitting analysis that the average valence state of Pd species in the Pd@Ce-BTC-N, Pd/Ce-BTC-N, Pd@Ce-BTC-A, Pd/Ce-BTC-A, and Pd/CeO_2 catalysts was 0.1, 0.2, 1.7, 0.3, and 0.3, respectively (**Fig. S9** and **Table S3**). Such results further supported the conclusion that the Pd species in Pd@Ce-BTC-N, Pd/Ce-BTC-N, Pd/Ce-BTC-A, and Pd/CeO_2 catalysts were mainly in the form of Pd^0, while those in Pd@Ce-BTC-A were mainly in the form of $Pd^{\delta+}$ ($2 > \delta > 0$). Considering that the Pd@Ce-BTC-A, with $Pd^{\delta+}$, exhibited lower activity than Pd@Ce-BTC-N with metallic Pd, yet showed better performance than Pd/Ce-BTC-N, Pd/Ce-BTC-A, and Pd/CeO_2 in which Pd was primarily in metallic states, there was no direct correlation observed between the CO oxidation activity and the oxidation valence of Pd in this catalyst system. To investigate the coordination environment of Pd on different Pd-CeO_2 catalysts, the EXAFS curve fitting analysis was performed (Fig. 3**b** and **S10**, **Table S4**). The observation of Pd-Pd shell similar to that in Pd foil as well as the Pd-O and Pd-O-Pd shells similar to that in PdO on Pd@Ce-BTC-A indicated the formation of both Pd and PdO clusters/particles. The absence of Pd-O and Pd-O-Pd coordination shells and the inclusive presence of Pd-Pd coordination shell on Pd@Ce-BTC-N, Pd/Ce-BTC-N, Pd/Ce-BTC-A, and Pd/CeO_2 catalysts suggested that the Pd species on these catalysts were mainly in the form of metallic Pd clusters/particles.

3.4. Catalyst reducibility

CO-TPR experiment was conducted to investigate the redox properties of the Pd catalysts (Fig. 4). The CO-consumption peaks could be

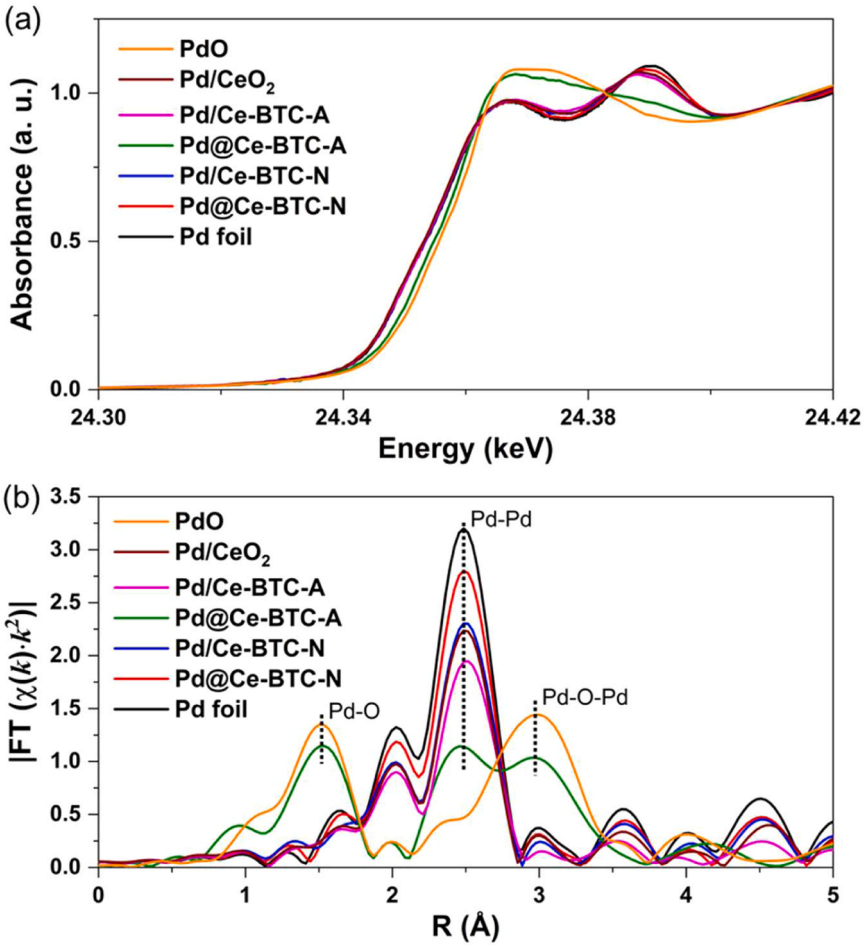

Fig. 3. (a) Normalized Pd K-edge XANES and (b) Fourier transformed k^2-weighted EXAFS oscillations in R space for Pd K-edge in Pd@Ce-BTC-N, Pd/Ce-BTC-N, Pd@Ce-BTC-A, Pd/Ce-BTC-A, and Pd/CeO_2 catalysts.

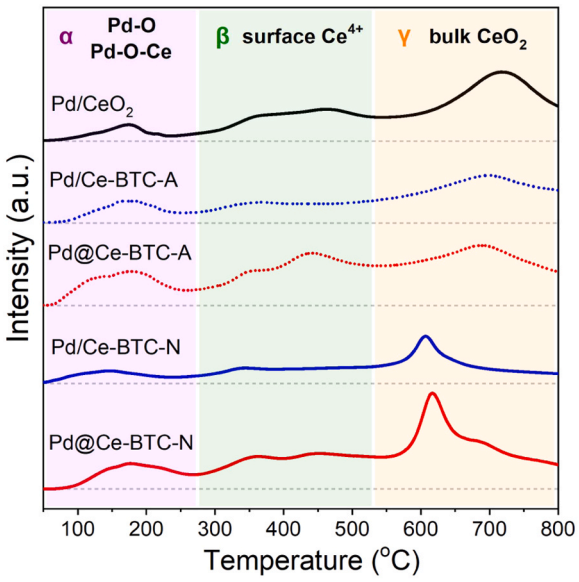

Fig. 4. CO-TPR profiles for Pd/CeO_2, Pd/Ce-BTC-A, Pd@Ce-BTC-A, Pd/Ce-BTC-N and Pd@Ce-BTC-N catalysts.

divided into three zones, and zone α (50–280 °C), zone β (280–530 °C) and zone γ (530–800 °C) could be assigned to the reduction of Pd-O/Pd-O-Ce, surface Ce^{4+} and bulk CeO_2, respectively.[10]; [31]; [33] Typically, the reducible species at low temperature range could play an important role in low temperature CO oxidation reaction. For Pd@Ce-BTC-N and Pd@Ce-BTC-A, the CO consumption peaks in zone α were much more intensive than those for Pd/CeO_2, Pd/Ce-BTC-N and Pd/Ce-BTC-A, suggesting the formation of more Pd-O and Pd-O-Ce species. This was further confirmed by the fact that a significantly higher relative CO consumption for the reduction of Pd-O/Pd-O-Ce species within Pd@Ce-BTC-N (11.5) and Pd@Ce-BTC-A (19.2) catalysts was observed comparing to that on other samples (5.1–8.2), as listed in **Table S5**. Considering the same loading of Pd on these catalysts, the formation of more Pd-O and Pd-O-Ce species could be resulted from the higher dispersion of Pd on Pd@Ce-BTC as suggested by the results of EDS-mapping. As previously reported, the dispersion state and the coordination environment of Pd species could play key roles in the CO oxidation reaction [12]; [20]; [23]; [31]. Our recent work also confirmed that the smaller Pd clusters on CeO_2-Al_2O_3 support exhibited better catalytic performance in CO/hydrocarbon oxidation reactions [31]. Therefore, the higher dispersion of Pd along with the superior low-temperature redox ability should have contributed to the higher CO oxidation activity on catalysts derived from Pd@Ce-BTC than those from Pd/Ce-BTC.

3.5. Oxygen vacancy and oxygen species

Fig. 5**a** shows the Ce 3d XPS of all the catalysts, and the

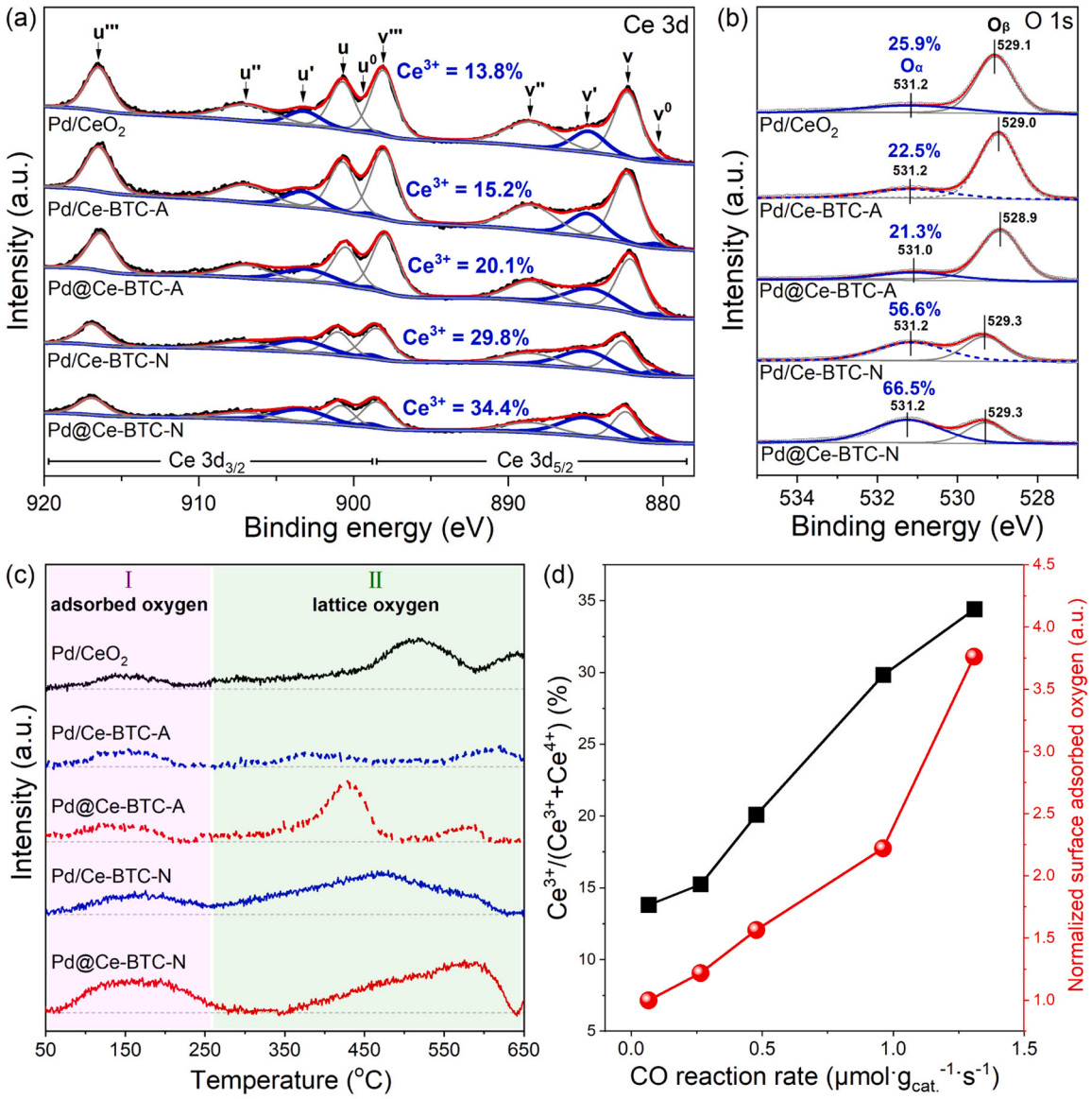

Fig. 5. (a) Ce 3d XPS, (b) O 1 s XPS, and (c) O_2-TPD profiles for Pd/CeO_2, Pd/Ce-BTC-A, Pd@Ce-BTC-A, Pd/Ce-BTC-N, and Pd@Ce-BTC-N catalysts. (d) The relationship between CO reaction rate (at 100 °C) and surface Ce^{3+} concentration as well as the normalized surface adsorbed oxygen species (the amount of surface adsorbed oxygen species on Pd/CeO_2 was normalized to 1).

concentration of surface Ce^{3+} was calculated based on the fitting results [21]. All catalysts derived from Pd/Ce-BTC and Pd@Ce-BTC showed higher concentration of surface Ce^{3+} than Pd/CeO_2. Furthermore, more Ce^{3+} species were observed on Pd/Ce-BTC-N (29.8%) and Pd@Ce-BTC-N (34.4%), which should be related to the lower crystallinity of CeO_2 supports with more oxygen vacancies. As widely reported, the higher concentration of surface Ce^{3+} could be beneficial for the adsorption and activation of oxygen, which therefore contributed to the improvement of catalytic oxidation performance [27]. The O 1 s XPS for all the catalysts were also collected and are illustrated in Fig. 5**b**. Peak O_α and peak O_β were assigned to the surface adsorbed oxygen species and the lattice oxygen species, respectively [15]; [25]. As expected, much more surface adsorbed oxygen species were observed on Pd/Ce-BTC-N (56.6%) and Pd@Ce-BTC-N (66.5%) than on Pd/Ce-BTC-A (22.5%), Pd@Ce-BTC-A (21.3%), and Pd/CeO_2 (25.9%), indicating that the catalysts obtained in N_2 atmosphere showed better capacity in the adsorption and activation of O_2. As previously demonstrated, the abundant surface adsorbed oxygen species could further facilitate the oxidation of CO, well explaining why the Pd/Ce-BTC-N and Pd@Ce-BTC-N catalysts showed higher CO oxidation activity than Pd/Ce-BTC-A, Pd@Ce-BTC-A, and Pd/CeO_2 counterparts. The relatively higher ratio of surface adsorbed oxygen species on Pd@Ce-BTC-N (66.5%) than that on Pd/Ce-BTC-N (56.6%) accounted for the higher CO oxidation activity achieved on the former catalyst.

O_2-TPD was conducted to further investigate the oxygen adsorption-desorption properties of Pd catalysts. As illustrated in Fig. 5**c**, two sets of oxygen desorption peaks could be observed on all catalysts. The peak I could be attributed to the desorption of oxygen species adsorbed on the surface of the catalysts, which were highly active in catalytic oxidation reactions, while peak II could be assigned to the desorption of lattice oxygen. The normalized area of peak I was calculated and listed in **Table S1**, in which the amount of surface adsorbed oxygen species on Pd/CeO_2 reference was normalized to 1. It was noticeable that the peak I on Pd@Ce-BTC-N was much more intensive than those on other Pd catalysts, suggesting the presence of a much higher amount of surface adsorbed oxygen species on Pd@Ce-BTC-N. The results of O_2-TPD well supported the observation in O 1 s XPS that more surface oxygen species were formed on Pd@Ce-BTC-N. As reported by Chen *et al.*, for Pd-CeO_2

catalyst, the enriched surface Ce^{3+} and oxygen vacancies could facilitate the activation of O_2 to generate surface active oxygen species, which then effectively reacted with CO adsorbed on Pd sites [5]. To better reveal the relationship between surface Ce^{3+} concentrations, the amount of surface adsorbed oxygen species and the CO oxidation activity on these catalysts, the plots of $Ce^{3+}/(Ce^{3+} + Ce^{4+})$ ratio and the normalized surface adsorbed oxygen versus the CO reaction rate are presented in Fig. 5**d**. It was evident that the CO oxidation activity on the serial Pd-Ce-BTC derived catalysts was indeed strongly correlated to the surface Ce^{3+} concentrations and surface adsorbed oxygen. The higher concentration of surface Ce^{3+} and more abundant surface adsorbed oxygen species on Pd@Ce-BTC-N significantly contribute to its superior CO oxidation activity at low temperatures.

4. Conclusions

There is always urgent demand for simpler and more environmental-friendly preparation methods for catalytic materials, along with the enhancement of low-temperature catalytic activity. In this work, a facile one-pot solvothermal synthesis method was developed for the preparation of Pd catalysts incorporated into the CeO_2 derived from Ce-BTC (Pd@Ce-BTC). Comparing to the catalysts derived from Pd/Ce-BTC prepared by the conventional method, those derived from Pd@Ce-BTC via the one-pot solvothermal approach exhibited higher Pd dispersion and significantly improved the catalytic performance in CO oxidation. Additionally, the pyrolysis treatment conducted in N_2 flow proved to be more favorable for obtaining more efficient Pd-CeO_2 catalyst comparing to the pyrolysis treatment in air flow. Among all the investigated catalysts, the Pd@Ce-BTC-N pyrolyzed in N_2 flow showed exceptional catalytic activity for CO oxidation, due to its higher Pd dispersion and more surface Ce^{3+} species and adsorbed oxygen species. This work provides an instructive strategy for the preparation of metal-MOF materials and their derived catalysts aimed at the more effective control of industrial or automotive emissions.

Environmental Implication

Precious metal catalysts derived from metal-organic frameworks (MOFs) have attracted considerable attention in environmental catalysis. However, the preparation of precious metal catalysts supported by MOFs typically involves multiple steps. Herein, we developed a novel one-pot solvothermal method for the preparation of Pd incorporated in Ce-BTC (Pd@Ce-BTC). The Pd-CeO_2 catalyst, derived from the one-pot generated Pd@Ce-BTC exhibited superior CO oxidation activity comparing to the reference catalyst derived from Pd/Ce-BTC prepared through a conventional two-step method. This study offers an instructive strategy for preparing metal-MOF materials and their derived catalysts for potential emission control applications.

CRediT authorship contribution statement

Shaohua Xie: Writing – review & editing, Writing – original draft, Visualization, Investigation. **Wei Tan:** Writing – review & editing, Writing – original draft, Visualization, Investigation. **Yuhan Xu:** Visualization, Investigation, Formal analysis. **Chunying Wang:** Investigation, Formal analysis. **Yuan Feng:** Investigation, Formal analysis. **Kailong Ye:** Investigation, Formal analysis. **Lu Ma:** Resources, Investigation. **Steven N. Ehrlich:** Resources, Investigation. **Yaobin Li:** Resources, Investigation. **Yan Zhang:** Resources, Investigation. **Lin Dong:** Resources, Investigation. **Jiguang Deng:** Writing – review & editing, Supervision, Funding acquisition, Conceptualization. **Fudong Liu:** Writing – review & editing, Supervision, Funding acquisition, Conceptualization.

Declaration of Competing Interest

The authors declare that they have no known competing financial interests or personal relationships that could have appeared to influence the work reported in this paper.

Data Availability

Data will be made available on request.

Acknowledgement

This work was supported by the Startup Fund (F. L.) from the University of Central Florida (UCF), the University of California, Riverside (UCR) and the NSF-PREM grant (DMR-2121953). J. D. thanks the support from National Natural Science Foundation of China (22106007), Key Science and Technology Projects of Beijing Municipal Education Commission (KZ202210005011), and Natural Science Foundation of Hebei Province (B2021208033). S. X. thanks the support from the Pre-eminent Postdoctoral Program (P3) at UCF. W. T. thanks the support from National Natural Science Foundation of China (22306090). This research used beamline 7-BM (QAS) of the National Synchrotron Light Source II (NSLS-II), a U.S. Department of Energy (DOE) Office of Science User Facility operated for the DOE Office of Science by Brookhaven National Laboratory (BNL) under Contract No. DE-SC0012704.

Appendix A. Supporting information

Supplementary data associated with this article can be found in the online version at doi:10.1016/j.jhazmat.2024.133632.

References

[1] An, B., Zhang, J., Cheng, K., Ji, P., Wang, C., Lin, W., 2017. Confinement of ultrasmall Cu/ZnO_x nanoparticles in metal–organic frameworks for selective methanol synthesis from catalytic hydrogenation of CO_2. J Am Chem Soc 139 (10), 3834–3840. https://doi.org/10.1021/jacs.7b00058.

[2] Cai, D., Chen, B., Huang, Z., Zeng, X., Xiao, J., Zhou, S.F., et al., 2021. Metal oxide/CeO_2 nanocomposites derived from Ce-benzene tricarboxylate (Ce-BTC) adsorbing with metal acetylacetonate complexes for catalytic oxidation of carbon monoxide. RSC Adv 11 (34), 21057–21065. https://doi.org/10.1039/d1ra03319k.

[3] Carpenter, M.K., Moylan, T.E., Kukreja, R.S., Atwan, M.H., Tessema, M.M., 2012. Solvothermal synthesis of platinum alloy nanoparticles for oxygen reduction electrocatalysis. J Am Chem Soc 134 (20), 8535–8542. https://doi.org/10.1021/ja300756y.

[4] Chen, B., Zeng, X., Liu, Y., Xiao, F., Huang, M., Bing Tan, K., et al., 2022. Thermal decomposition kinetics of *M*−BTC (*M* = Cu, Co, Zn, and Ce) and M−BTC/Pt composites under oxidative and reductive environments. Chem Eng J 450, 138470. https://doi.org/10.1016/j.cej.2022.138470.

[5] Chen, Y., Chen, J., Qu, W., George, C., Aouine, M., Vernoux, P., et al., 2018. Well-defined palladium–ceria interfacial electronic effects trigger CO oxidation. Chem Commun 54 (72), 10140–10143. https://doi.org/10.1039/C8CC04935A.

[6] Chughtai, A.H., Ahmad, N., Younus, H.A., Laypkov, A., Verpoort, F., 2015. Metal–organic frameworks: versatile heterogeneous catalysts for efficient catalytic organic transformations. Chem Soc Rev 44 (19), 6804–6849. https://doi.org/10.1039/C4CS00395K.

[7] Fan, L., Wang, K., Xu, K., Liang, Z., Wang, H., Zhou, S.F., et al., 2020. Structural isomerism of two Ce-BTC for fabricating Pt/CeO_2 nanorods toward low-temperature CO oxidation. Small 16 (40), e2003597. https://doi.org/10.1002/smll.202003597.

[8] Fan, L., Zhao, F., Huang, Z., Chen, B., Zhou, S.-F., Zhan, G., 2019. Partial deligandation of M/Ce-BTC nanorods (M = Au, Cu, au-cu) with "Quasi-MOF" structures towards improving catalytic activity and stability. Appl Catal A: Gen 572, 34–43. https://doi.org/10.1016/j.apcata.2018.12.021.

[9] Freund, R., Zaremba, O., Arnauts, G., Ameloot, R., Skorupskii, G., Dinca, M., et al., 2021. The current status of MOF and COF applications. Angew Chem Int Ed 60 (45), 23975–24001. https://doi.org/10.1002/anie.202106259.

[10] Hu, Z., Liu, X., Meng, D., Guo, Y., Guo, Y., Lu, G., 2016. Effect of ceria crystal plane on the physicochemical and catalytic properties of Pd/ceria for CO and propane oxidation. ACS Catal 6 (4), 2265–2279. https://doi.org/10.1021/acscatal.5b02617.

[11] Ikuno, T., Zheng, J., Vjunov, A., Sanchez-Sanchez, M., Ortuño, M.A., Pahls, D.R., et al., 2017. Methane oxidation to methanol catalyzed by Cu-Oxo clusters stabilized in NU-1000 metal–organic framework. J Am Chem Soc 139 (30), 10294–10301. https://doi.org/10.1021/jacs.7b02936.

[12] Jeong, H., Bae, J., Han, J.W., Lee, H., 2017. Promoting effects of hydrothermal treatment on the activity and durability of Pd/CeO_2 catalysts for CO oxidation. ACS Catal 7 (10), 7097–7105. https://doi.org/10.1021/acscatal.7b01810.
[13] Kar, A.K., Kaur, S.P., Kumar, T.J.D., Srivastava, R., 2020. Efficient hydrogenolysis of aryl ethers over Ce-MOF supported Pd NPs under mild conditions: mechanistic insight using density functional theoretical calculations. Catal Sci Technol 10 (20), 6892–6901. https://doi.org/10.1039/d0cy01279c.
[14] Konnerth, H., Matsagar, B.M., Chen, S.S., Prechtl, M.H.G., Shieh, F.-K., Wu, K.C.W., 2020. Metal-organic framework (MOF)-derived catalysts for fine chemical production. Coord Chem Rev 416, 213319. https://doi.org/10.1016/j.ccr.2020.213319.
[15] Liu, F., Shan, W., Lian, Z., Liu, J., He, H., 2018. The smart surface modification of Fe_2O_3 by WO_x for significantly promoting the selective catalytic reduction of NO_x with NH_3. Appl Catal, B 230, 165–176. https://doi.org/10.1016/j.apcatb.2018.02.052.
[16] Liu, Y., Jie, W., Liu, F., Liu, Q., Qiu, M., Gong, X., et al., 2023. Effect of Ce-BTC precursor morphology on CuO/CeO_2 catalysts for CO preferential oxidation in H_2-rich gas. Solid State Sci 139, 107182. https://doi.org/10.1016/j.solidstatesciences.2023.107182.
[17] Loridant, S., 2021. Raman spectroscopy as a powerful tool to characterize ceria-based catalysts. Catal Today 373, 98–111. https://doi.org/10.1016/j.cattod.2020.03.044.
[18] Maiti, S., Pramanik, A., Mahanty, S., 2014. Extraordinarily high pseudocapacitance of metal organic framework derived nanostructured cerium oxide. Chem Commun 50 (79), 11717–11720. https://doi.org/10.1039/C4CC05363J.
[19] Nie, L., Mei, D., Xiong, H., Peng, B., Ren, Z., Hernandez, X.I.P., et al., 2017. Activation of surface lattice oxygen in single-atom Pt/CeO_2 for low-temperature CO oxidation. Science 358, 1419–1423. https://doi.org/10.1126/science.aao2109.
[20] Priolkar, K.R., Bera, P., Sarode, P.R., Hegde, M.S., Emura, S., Kumashiro, R., et al., 2002. Formation of $Ce_{1-x}Pd_xO_{2-\delta}$ solid solution in combustion-synthesized Pd/CeO_2 catalyst: XRD, XPS, and EXAFS investigation. Chem Mater 14 (5), 2120–2128. https://doi.org/10.1021/cm0103895.
[21] Qi, L., Yu, Q., Dai, Y., Tang, C., Liu, L., Zhang, H., et al., 2012. Influence of cerium precursors on the structure and reducibility of mesoporous CuO-CeO_2 catalysts for CO oxidation. Appl Catal, B 119-120, 308–320. https://doi.org/10.1016/j.apcatb.2012.02.029.
[22] Ranocchiari, M., Bokhoven, J.Av, 2011. Catalysis by metal–organic frameworks: fundamentals and opportunities. Phys Chem Chem Phys 13 (14), 6388–6396. https://doi.org/10.1039/C0CP02394A.
[23] Spezzati, G., Su, Y., Hofmann, J.P., Benavidez, A.D., DeLaRiva, A.T., McCabe, J., et al., 2017. Atomically dispersed Pd–O species on CeO_2(111) as highly active sites for low-temperature CO oxidation. ACS Catal 7 (10), 6887–6891. https://doi.org/10.1021/acscatal.7b02001.
[24] Su, C., Li, Z., Mao, M., Ye, W., Zhong, J., Ren, Q., et al., 2022. Unraveling specific role of carbon matrix over Pd/quasi-Ce-MOF facilitating toluene enhanced degradation. J Rare Earths 40 (11), 1751–1762. https://doi.org/10.1016/j.jre.2021.09.017.
[25] Tan, W., Wang, J., Li, L., Liu, A., Song, G., Guo, K., et al., 2020. Gas phase sulfation of ceria-zirconia solid solutions for generating highly efficient and SO_2 resistant NH_3-SCR catalysts for NO removal. J Hazard Mater 388, 121729. https://doi.org/10.1016/j.jhazmat.2019.121729.
[26] Tan, W., Xie, S., Le, D., Diao, W., Wang, M., Low, K.B., et al., 2022. Fine-tuned local coordination environment of Pt single atoms on ceria controls catalytic reactivity. Nat Commun 13 (1), 7070. https://doi.org/10.1038/s41467-022-34797-2.
[27] Tan, W., Xie, S., Wang, X., Wang, C., Li, Y., Shaw, T.E., et al., 2021. Highly efficient Pt catalyst on newly designed CeO_2-ZrO_2-Al_2O_3 support for catalytic removal of pollutants from vehicle exhaust. Chem Eng J 426, 131855. https://doi.org/10.1016/j.cej.2021.131855.
[28] Wang, Q., Astruc, D., 2020. State of the art and prospects in metal-organic framework (MOF)-based and MOF-derived nanocatalysis. Chem Rev 120 (2), 1438–1511. https://doi.org/10.1021/acs.chemrev.9b00223.
[29] Xie, S., Liu, L., Lu, Y., Wang, C., Cao, S., Diao, W., et al., 2022. Pt atomic single-layer catalyst embedded in defect-enriched ceria for efficient CO oxidation. J Am Chem Soc 144 (46), 21255–21266. https://doi.org/10.1021/jacs.2c08902.
[30] Xie, S., Liu, Y., Deng, J., Zhao, X., Yang, J., Zhang, K., et al., 2016. Three-dimensionally ordered macroporous CeO_2-supported Pd@Co nanoparticles: Highly active catalysts for methane oxidation. J Catal 342, 17–26. https://doi.org/10.1016/j.jcat.2016.07.003.
[31] Xie, S., Wang, Z., Tan, W., Zhu, Y., Collier, S., Ma, L., et al., 2021. Highly active and stable palladium catalysts on novel ceria–alumina supports for efficient oxidation of carbon monoxide and hydrocarbons. Environ Sci Technol 55 (11), 7624–7633. https://doi.org/10.1021/acs.est.1c00077.
[32] Xiong, H., Kunwar, D., Jiang, D., García-Vargas, C.E., Li, H., Du, C., et al., 2021. Engineering catalyst supports to stabilize PdO_x two-dimensional rafts for water-tolerant methane oxidation. Nat Catal 4 (10), 830–839. https://doi.org/10.1038/s41929-021-00680-4.
[33] Ye, J., Xia, Y., Cheng, D.-g, Chen, F., Zhan, X., 2019. Promoting effects of pretreatment on Pd/CeO_2 catalysts for CO oxidation. Int J Hydrog Energy 44 (33), 17985–17994. https://doi.org/10.1016/j.ijhydene.2019.05.099.
[34] Zhang, X., Bi, F., Zhu, Z., Yang, Y., Zhao, S., Chen, J., et al., 2021. The promoting effect of H_2O on rod-like $MnCeO_x$ derived from MOFs for toluene oxidation: a combined experimental and theoretical investigation. Appl Catal B: Environ 297, 120393. https://doi.org/10.1016/j.apcatb.2021.120393.
[35] Zhang, X., Zhang, X., Song, L., Hou, F., Yang, Y., Wang, Y., et al., 2018. Enhanced catalytic performance for CO oxidation and preferential CO oxidation over CuO/CeO_2 catalysts synthesized from metal organic framework: effects of preparation methods. Int J Hydrog Energy 43 (39), 18279–18288. https://doi.org/10.1016/j.ijhydene.2018.08.060.
[36] Zhang, Z., Tian, J., Lu, Y., Yang, S., Jiang, D., Huang, W., et al., 2023. Memory-dictated dynamics of single-atom Pt on CeO_2 for CO oxidation. Nat Commun 14 (1), 2664. https://doi.org/10.1038/s41467-023-37776-3.